JOURNAL OF AIRCRAFT
Vol. 49, No. 4, July–August 2012

Ship–Helicopter Operating Limits Prediction Using Piloted Flight Simulation and Time-Accurate Airwakes

James S. Forrest*
Prism Defence Pty., Ltd., North Adelaide 5006, South Australia, Australia
Ieuan Owen†
University of Lincoln, Lincoln LN6 7TS, England, United Kingdom
Gareth D. Padfield‡
University of Liverpool, Liverpool L69 3BX, England, United Kingdom
and
Steven J. Hodge§
BAE Systems, Preston PR4 1AX, England, United Kingdom

DOI: 10.2514/1.C031525

This paper gives an overview of the ship–helicopter dynamic interface simulation facility at the University of Liverpool, with an emphasis on recent improvements made through the inclusion of unsteady computational fluid dynamics (CFD) ship airwake data. A FLIGHTLAB model of an SH-60B Seahawk helicopter has been flown in a full motion base simulator to the deck of a Type 23 frigate and a Wave class auxiliary oiler, under the influence of unsteady airwakes derived from CFD. Pilot workload ratings have been obtained for the deck landing task, using both the Bedford workload rating scale and the deck interface pilot effort scale, from which fully simulated ship–helicopter operating limits have been derived. Analysis of pilot ratings, comments, and control inputs has also enabled both subjective and objective assessments of workloads at various wind-over-deck conditions, highlighting the dominant aerodynamic airwake features which contribute to the difficulty of the landing task. Having access to the underlying CFD data allows the aircraft handling qualities and pilot workload to be correlated with the aerodynamic characteristics of the airwake and identification of the geometric features of the ship that cause them.

I. Introduction

LANDING a helicopter on to the flight deck of a ship can be a formidable task for even the most experienced of pilots. The difficulties associated with the landing task arise due to several environmental factors which are unique to the maritime environment. Sea swell leads to movement of the ship about its principal degrees of freedom (pitch, roll and heave), effectively making the landing spot a moving target; at the same time, air passing over the ship's superstructure forms large-scale turbulent eddies which pass over the landing deck and perturb the aircraft during approach. This region of disturbed flow is known as the ship's airwake, and its severity is dependent on the atmospheric wind speed, the ship's forward speed and the relative wind-over-deck (WOD) angle. The close proximity of the helicopter to the ship during landing makes this a high-risk maneuver and as both the ship motion and the ship airwake are responsible for increasing pilot workload, it is necessary to develop ship–helicopter operating limits (SHOL) to minimize the risk of accidents.

Figure 1 shows a typical SHOL diagram, with the relative WOD direction (where the wind is coming from) around the circumference and the WOD speed on the radial axis. In accordance with naval terminology, winds from the starboard side are termed "green" and those from port termed "red." The SHOL boundary is the thick black line which encloses all points that are deemed safe for repeated landings. For example, at a 40° WOD angle the maximum allowable WOD speed would be 35 kt. Landings at conditions outside the boundary are not normally permitted, except in extreme circumstances. Furthermore, during operations (for example if the ship is part of a flotilla or is patrolling near the coast) it is not always possible for a ship to turn to give the incoming pilot a favorable WOD condition, so it is always operationally advantageous to maximize the SHOL envelope.

In the United Kingdom, the Royal Navy (RN) requires SHOL boundaries for each in-service ship–helicopter combination, with additional charts needed for day/night operations and different aircraft weights [1]. The first-of-class flight trials (FOCFT) which are used to determine the SHOL boundaries are performed over a limited time period, typically several weeks, and are at the mercy of the weather; as a result, it is usually impossible to obtain test points at every desired combination of WOD speed and angle. This often leads to overly conservative SHOLs that are limited by scheduling and meteorological constraints, rather than by aircraft or pilot limits. Furthermore, at-sea SHOL testing is inherently hazardous due to the fact that pilots are operating close to their own limits, as well as those of the aircraft. Finally, the dedicated use of naval hardware during SHOL testing ties up helicopters, ships, and personnel for significant periods of time, diverting resources from their primary operational roles.

For the reasons described previously, it has been suggested that modeling and simulation of the ship–helicopter dynamic interface (DI) may be used to augment the SHOL definition process [2]. Potential benefits offered by DI simulation include 1) identification of WOD "hot spots" before at-sea testing which can be used to inform the flight-test program; 2) the ability to assess particular WOD conditions which may have been missed during at-sea testing in order to maximize the operational envelope; 3) investigation of flight deck aerodynamics while new ships are still at the design stage to identify potential improvements to superstructure design, landing spot locations and placement of equipment; 4) a greater understanding of ship airwake turbulence and the mechanisms which cause it; and 5) a realistic simulation environment in which to conduct pilot training exercises.

Received 27 May 2011; revision received 8 September 2011; accepted for publication 10 October 2011.

*Senior Fluids Engineer; james.forrest@prismdefence.com (Corresponding Author).
†Professor of Mechanical Engineering, School of Engineering.
‡Professor of Aerospace Engineering, Department of Engineering.
§Senior Simulation Engineer, Flight Simulation Department.

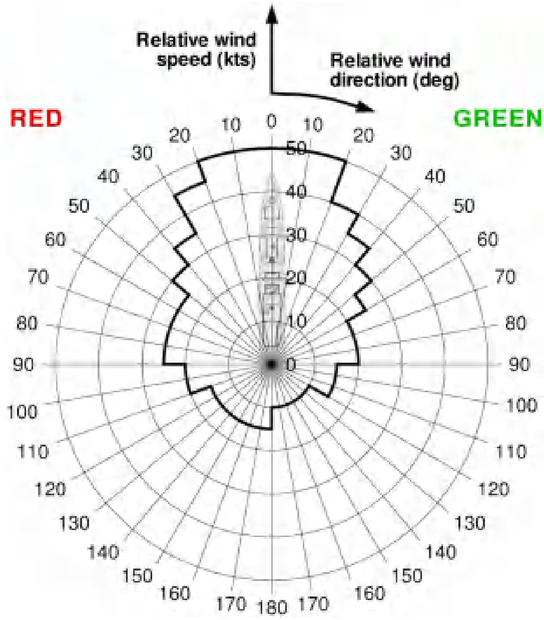

Fig. 1 A typical SHOL diagram.

A great deal of DI modeling and simulation effort has focused on improving the fidelity of piloted flight simulators such that the results from simulated SHOL trials are comparable to those from at-sea flight trials. Indeed, significant progress towards this goal has been made by naval operators in the United Kingdom, United States, and Australia in recent years [3–8]. One aspect of DI modeling which has been identified as particularly important with regards to improving fidelity is the ship airwake [9]. Much of the pilot workload experienced during landing is a direct result of disturbances caused by the airwake, so it follows that accurate modeling of the airwake is a key step in replicating appropriate levels of workload in any DI simulation.

Blackwell et al. [3] and, later, Erm [4] from the Australian Defence Science and Technology Organisation presented one early example of an SH60B/FFG-7 frigate simulation capability, which was based on aerodynamic ship airwake data obtained from wind-tunnel tests on a model frigate. Significant differences were found between airwake velocities predicted by the model and those measured during at-sea tests. The discrepancies were attributed to the use of a wind-tunnel model whose superstructure was not sufficiently similar to the FFG-7. In addition, simplifications within the helicopter model such as the use of an actuator disk rotor model and the assumption that the airwake velocity at the aircraft center of gravity could be applied over the entire aircraft were identified as deficiencies which required attention. It was recommended that a blade element rotor model which could detect velocity gradients across the rotor would improve the effectiveness of the simulation.

As part of a review of collaborative DI modeling activities, Wilkinson et al. [5] described the development of a ship–helicopter simulation facility based at the United Kingdom's Defence Evaluation and Research Agency. The airwake module was based on the superposition of basic flow patterns, with turbulent fluctuations provided by scaled random velocity time histories. Because of the empirical nature of this airwake database, the three-dimensional components of turbulence were not correlated.

From the late 1990s the improvement in computational fluid dynamics (CFD) codes and availability of high-performance computing facilities meant that ship airwake modeling activities increasingly moved from the wind tunnel to computer simulations. Several researchers have published computational studies on ship airwake aerodynamics [10–25], with the results from Polsky [17], Lee et al. [20], Roper et al. [23] and Forrest and Owen [25] being used to populate look-up tables for shipboard flight simulator investigations.

Bunnell [6] and Roscoe and Thompson [7] presented details of a CFD-based shipboard helicopter flight simulation facility in the Vertical Motion Simulator, located at the NASA Ames Research Center, which was developed as part of the U.S. Joint Shipboard Helicopter Integration Process program. The DI Modeling and Simulation System was configured such that the fidelity levels of the various subsystems could be altered to give an overall fidelity configuration between level A and D, with level A corresponding to full motion base, seat shaker, and high-performance image generator with high-fidelity visual models. A series of simulated UH-60/LHA deck landings were performed by several pilots, with results compared to flight-test data which had been recorded during at-sea landings. Using the five-point deck interface pilot effort scale (DIPES) to rate the difficulty of the deck landings it was found that, compared with the at-sea tests, mean DIPES ratings in the simulator were within 1 point of the corresponding ratings awarded at sea. However, the simulated SHOL was greatly expanded in comparison with the real SHOL, largely due to the fact that insufficient high-workload WOD conditions were encountered during sea trials due to benign environmental conditions. This was highlighted as further evidence of the need for high-fidelity piloted simulation capability.

The most recent example of a piloted ship–helicopter DI simulation environment was presented by Cox and Duncan [8], who described the United Kingdom's Ship–Air Interface Framework project. Using a networked "high-level architecture" simulation with time-accurate ship airwake data (some of which was contributed by the current authors), piloted simulation flight trials were conducted for a Merlin helicopter to RN ships including the Type 23 frigate, Wave class auxiliary oiler (AO) and Type 45 destroyer. It was found that moving from a steady-state CFD-based airwake database with statistical turbulence modeling to a time-accurate database provided more realistic turbulent fluctuations, with an improved match between the simulated and at-sea flight-test ratings.

To date, the common approach for CFD-based ship–helicopter flight simulators has been for the ship airwake computations to be performed elsewhere; either in a separate department or by contracting out to other organizations. There is very little evidence in the literature to suggest that DI simulation researchers have examined simulated flight trial results in the context of the underlying aerodynamic airwake data. Given the wealth of information held within the CFD datasets, it is possible that researchers are missing opportunities to gain real insight into the nature of ship airwake turbulence and its impact on helicopter flight dynamics. A better understanding of airwake turbulence and its role in driving pilot workload during ship–helicopter operations presents opportunities for improving the design of ship superstructures and augmented flight control systems, both of which should lead to improved safety and expanded operational capability.

This paper presents the results of a series of piloted flight simulation trials in which an SH-60B Sea Hawk helicopter has been flown to the deck of several different ships, under the influence of unsteady CFD-based ship airwakes. Both the CFD computations [25,26] and the flight trials [24,27] have been conducted by the current authors, whereby a key part of the analysis has been returning to the CFD data to understand and explain various phenomena observed during deck landings. Pilot workload ratings have been used to derive, as far as the authors are aware, the first fully simulated SHOL diagrams published in the literature.

The first part of the paper describes the simulator facility, before details of the CFD airwake generation and integration are given. Next, results from the flight trials are presented, in terms of control activity, pilot workload ratings and SHOL diagrams. Finally, some of the underlying CFD airwake data are shown in order to explain certain results from the flight trials.

II. Ship–Helicopter Simulation Approach

A. HELIFLIGHT-R Flight Simulation Facility

Piloted flight trials were conducted in the University of Liverpool's HELIFLIGHT-R flight simulation facility, shown in Fig. 2. The facility consists of a six-degree-of-freedom, full motion base simulator, driven by several Linux-based PCs running FLIGHTLAB aircraft models through the PilotStation software

a) b)

Fig. 2 The HELIFLIGHT-R flight simulator: a) external view and b) internal view.

package. The simulator itself is electrically actuated and capable of peak accelerations up to ± 1.0 g in heave and ± 0.7 g in surge and sway. HELIFLIGHT-R has been used successfully in a number of rotorcraft and fixed-wing simulation research projects [28,29]. During the ship–helicopter trials the simulator was configured in a side-by-side, two-seat helicopter arrangement, with visuals provided by three LCD projectors giving a 220 by 65 deg field of view. Because of the 12 ft projection dome, visuals are projected on to a region close to the pilot's feet, however, there are no discrete chin windows.

A FLIGHTLAB model of a UH-60 helicopter was used during the current study, with the location of its rear tail-wheel modified to make it representative of an SH-60B Seahawk (Fig. 3). Forces and moments on the four-bladed main rotor were calculated using a blade element model, with a finite-state dynamic inflow model used to account for distortion of air flow into the rotor disk. The tail rotor was modeled as a Bailey rotor disk, described in more detail in [30]. Forces on the fuselage and empennage were calculated from look-up tables of lift, drag and moment coefficients based on local flow velocities.

Fig. 5 Image of the Wave class AO (left) and Type 23 frigate (right) side by side.

B. Computational Fluid Dynamics Ship Airwake Model

Time-accurate CFD computations of the simple frigate shape (SFS2) research geometry, Type 23 frigate (T23), and Wave class AO were performed using the FLUENT finite volume solver. The detached-eddy simulation (DES) turbulence modeling approach was used [31], enabling the explicit capture of medium to large-scale turbulent structures in refined regions of the mesh. The CAD geometries of the ships are shown in Fig. 4, with images of the T23 and AO also shown for reference in Fig. 5 (it is worth noting the relative size of the ships, which will be shown later to play a factor in the difficulty of the simulated deck landings). A brief summary of the computational method is given next; a more detailed description and validation studies can be found in Forrest and Owen [25].

Each ship geometry was placed within an oval-shaped subdomain, in the center of a squat cylindrical domain, as shown in Fig. 6. This topology allowed the WOD angle to be changed simply by specifying the x and y components of velocity at the outer boundary, avoiding the need for remeshing. The cylinder was given a radius of approximately $r = 4.5 l_s$ and a depth of approximately $d = 0.75 l_s$, where l_s is ship length; this was sufficient to prevent the domain boundaries from affecting flow in the vicinity of the ship. Hybrid unstructured grids were created using a combination of the Gambit and T-grid meshing tools: using prism elements to capture the viscous boundary layer, tetrahedra within the oval subdomain, and

Fig. 3 An SH-60B Seahawk hovering over a frigate landing deck.

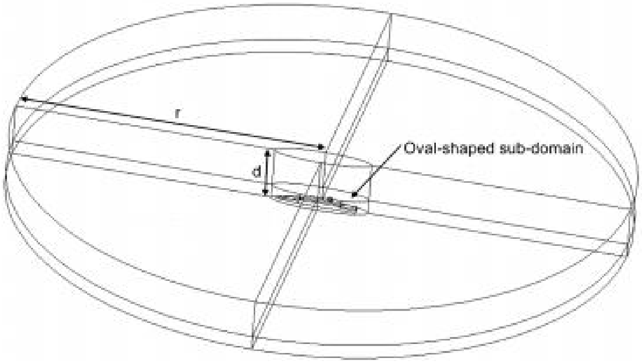

Fig. 6 The cylindrical mesh topology used for the CFD computations. The oval subdomain is indicated by an arrow.

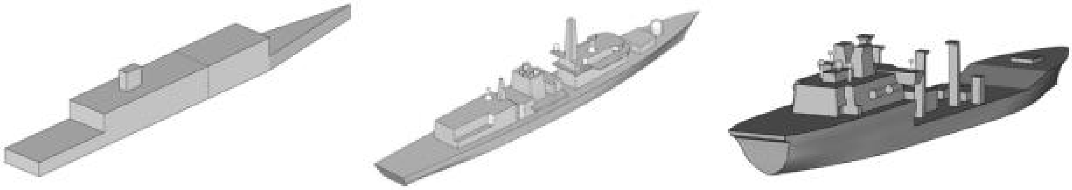

a) b) c)

Fig. 4 CAD geometry of the ships used for the CFD airwake computations: a) SFS2, b) Type 23 frigate, and c) Wave class AO.

Table 1 List of CFD airwakes generated for the airwake database. Indicated WOD speeds are defined at the ship anemometer height

Ship	WOD angles, deg	WOD speed	Velocity profile
SFS2	0, ±15, ±30, ±45, ±60, ±75, ±90	40 kt	Uniform
Type 23 frigate	0, ±15, ±30, ±45, ±60, ±90, ±135, 180	40, 37.5 kt	Uniform, ABL
Wave class AO	0, ±15, ±30, ±45, ±60, ±90, ±135, 180	39.8 kt	ABL

hexahedral cells throughout the rest of the domain. Size functions were employed to ensure gradual growth of cells away from the ship and also to create a refined region over the flight deck, in order to capture as wide a range of length scales as possible in this critical area. Cell counts were approximately 5.8×10^6, 7.4×10^6 and 8.4×10^6 for the SFS2, T23 and AO, respectively, reflecting the increasing geometric complexity and physical size of the ship geometries.

The curved cylindrical boundary was given a far-field boundary condition, with velocity specified in terms of x, y and z components. Runs were performed with uniform velocity profiles (as commonly seen in wind tunnels with boundary-layer removal) and also using power law profiles to model the effects of the Earth's atmospheric boundary layer (ABL) [32]. For the uniform flow cases the sea surface and the upper domain boundaries were given slip conditions; for the cases with ABL flow profiles the sea was modeled as a rough surface with wall functions and the upper domain boundary was modeled as a moving smooth wall with velocity equal to the wind at the boundary height. In all cases the ship surfaces were given a no-slip condition.

Each case was initiated using a steady-state solver, with the resulting velocity and turbulence fields used to initialize the time-accurate DES runs. After starting the unsteady solver, the solution was run for a period of 15 s before any airwake data or flow statistics were recorded; this was found to be sufficient time to initialize the solution. During the main computation phase the solver was run for a further 90 s, with the complete velocity field written to disk at each time-step, corresponding to a sampling rate of 80 Hz.

Given the high cell counts and the need for time-accurate DES computations, it was necessary to perform the CFD runs in parallel on the University of Liverpool's high-performance computing cluster. Each run was partitioned over 32 processing cores, allowing results to be obtained in approximately 8–10 days for each of the various cases. Typically several jobs were run concurrently to speed up the process.

To ensure that the airwake database contained sufficient flight conditions to develop a full SHOL envelope, computations were performed at a number of WOD conditions for each ship; these are shown in Table 1 for reference. The WOD angle is defined relative to the ship's bow and the WOD speed is defined at the ship anemometer height. Although the ABL computations for the T23 and the AO used the same velocity profile, the AO's anemometer is higher above the sea, leading to the higher WOD speed for the AO. Incidentally, the AO's flight deck is also higher above the sea than that of the T23, so true wind speeds at the deck are expected to be higher for the AO than the T23 for any given WOD condition.

C. Airwake Integration

The outcome of each of the CFD computations was a large number of data files consisting of velocity components at each grid point, with each data file corresponding to a different time within the time history. The data were not suitable for direct implementation into the HELIFLIGHT environment; partly due to formatting issues, but primarily due to the fact that the CFD output was unstructured. Therefore, a structured airwake grid was generated for each of the SFS2, T23 and AO ships. When designing these grids it was necessary to take into account the computational resources available in the simulator. Because of the FLIGHTLAB implementation, it was necessary to hold the full airwake time history in main memory (RAM). Through testing it was found that the maximum size of airwake data file which could be used without crashing the software was approximately 300 MB. The size of the airwake data file was a function of the update frequency, airwake length (in terms of time) and number of data points in the airwake grid; it was therefore necessary to strike a balance between these parameters to meet the 300 MB constraint.

With the preceding in mind, the airwake grids shown in Fig. 7 were constructed for the ships; the T23 grid shown in Fig. 7a was also used for the SFS2 flight tests as the two ships are very similar in size. Each grid used uniform 1 m spacing in each direction, giving cell counts of 18,000 and 32,062 for the T23 and AO, respectively. The AO required a larger domain than the T23 because it is a much bigger ship. The 1 m spacing was chosen as this allowed a large enough domain to conduct the deck landing task, while still providing a reasonable cell count. Each cell was similar in size to the blade section length on the main rotor blades and was small enough to provide a cell density which would allow large rotational airwake structures to be resolved on the grid.

The final airwake grids allowed airwake time histories of 30 and 22 s (with an update rate of 20 Hz) for the T23 and AO, respectively. It should be noted that the AO airwakes have not been validated against experimental data, because no suitable data were available at the time of these tests; however the computational method used to produce them was shown in Forrest and Owen [25] to give good agreement with wind-tunnel and full-scale data for the SFS2 and T23. The fact that the CFD method had been validated for two ships gave

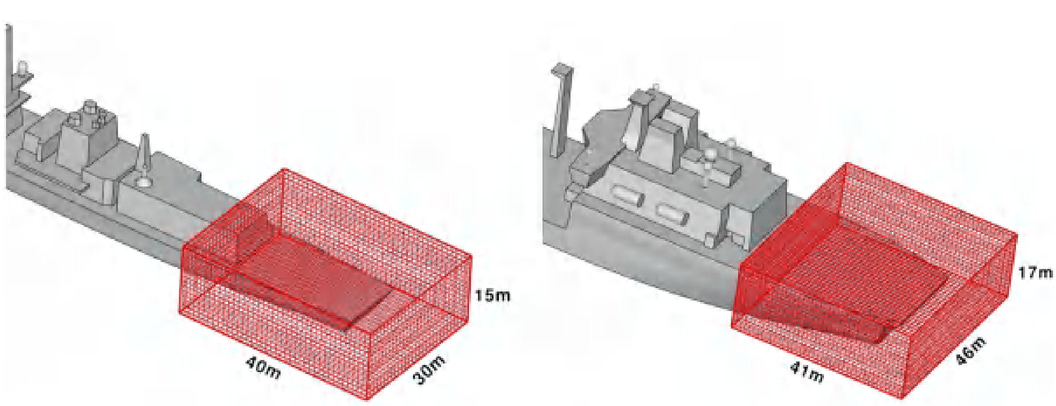

Fig. 7 Airwake output grids for the a) Type 23 frigate and b) Wave class AO.

confidence that the process could be used successfully for other geometries.

Once the airwake grids had been defined, the unstructured data were interpolated onto them using a linear interpolation routine. Finally, the resulting airwake data were converted into a format suitable for export to FLIGHTLAB using MATLAB scripts. Figure 8 shows a comparison of longitudinal velocity contours before and after interpolation on to the airwake grid, indicating that although some spatial resolution has been lost, the overall flow pattern remains the same.

During simulation the airwake database interacted with the aerodynamic surfaces (e.g., blade element, fuselage) by applying a time-varying velocity perturbation, based on the surface location and simulation time. The nature of the airwake/helicopter coupling was one-way; that is, the airwake perturbations affected the aircraft aerodynamics, but the aerodynamic forces (e.g., rotor inflow, downwash) did not, in turn, affect the airwake. Clearly, the true aerodynamic situation is a highly complex, fully coupled flowfield. However, until CFD computations of sufficient fidelity can be performed in real time, one-way coupling is the only feasible method for running piloted simulations with unsteady airwakes.

For each ship, the flowfield for each WOD angle was computed at only one WOD speed. Polsky [17] showed that, for typical WOD speeds, ship airwake data can be scaled linearly in terms of velocity magnitude, as the flow over bluff bodies at high Reynolds numbers is insensitive to moderate changes in Reynolds number (this was also tested and verified independently by the current authors using CFD). A value of approximately 40 kt WOD was chosen for all of the CFD runs as this WOD speed was expected to be in the middle of the SHOL envelope, meaning that the data would only have to be scaled moderately in both directions. The ability to scale airwake velocities resulted in a significant reduction in the required number of CFD computations, and provided a great deal of flexibility during simulator trials by allowing any given WOD speed to be specified. It should be noted that the WOD conditions tested represent a stationary ship, with all WOD generated by the freestream wind. At other combinations of wind/ship speeds, the incident wind profile changes due to a combination of the uniform "ship only" wind and the power law profile generated by the ABL. To simulate this correctly would have required a large number of additional CFD runs which was outside the scope of this project, although the phenomenon warrants further research.

D. Flight Trial Methodology

The deck landing trials were designed to mimic, as far as possible, the real SHOL derivation process used during FOCFT testing, with a highly experienced former RN test pilot employed to carry out the deck landings. The helicopter was given a mass of approximately 7400 kg, which is equivalent to a lightly loaded aircraft. All runs were performed at day, in good visibility, with ship motion equivalent to a sea state 4. The ship motion consisted of 5 min time histories of six-degree-of-freedom motion as recorded on board a RN aircraft carrier; this data had subsequently been scaled to make it more representative of a smaller frigate-sized vessel. The airwake grid was fixed relative to the ship, such that when the ship moved in pitch, roll or heave the airwake moved with it. This behavior was deemed preferable to keeping the airwake fixed relative to sea, as it was anticipated to be a more realistic representation of the real at-sea situation. However, the effect of ship motion on the airwake is not fully understood, and certainly warrants further investigation.

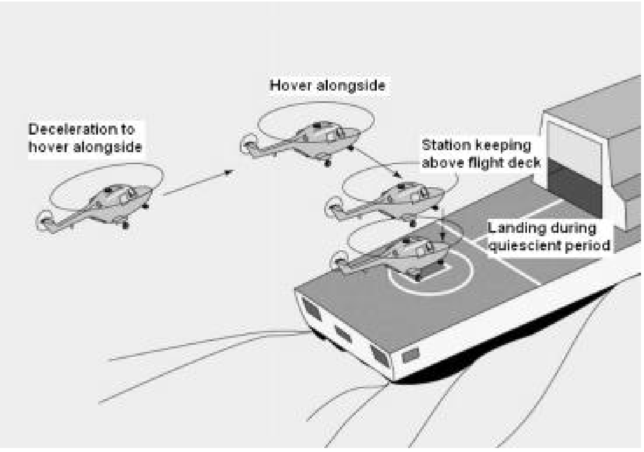

Fig. 9 Final stages of the recovery of a RN helicopter to a single-spot frigate.

Each deck landing sortie followed the standard RN deck landing approach [33] as illustrated in Fig. 9. This consists of an initial approach down the red 165 deg glide slope to a stabilized hover alongside the ship, followed by a lateral translation to hover over the landing spot, before finally making a vertical descent to touchdown. The full evolution was split into discrete mission task elements (MTEs), with an additional station keeping MTE added between the translation and landing MTEs. The station keeping MTE required the pilot to maintain the aircraft in a hover over the landing spot for a minimum of 10 s. This maneuver is not routinely performed during at-sea SHOL testing, but presented a valuable opportunity in which to gather data for analysis of pilot control activity in airwake turbulence. As the pilot was started off in a trimmed hover alongside the ship at the start of each sortie, the approach phase was not

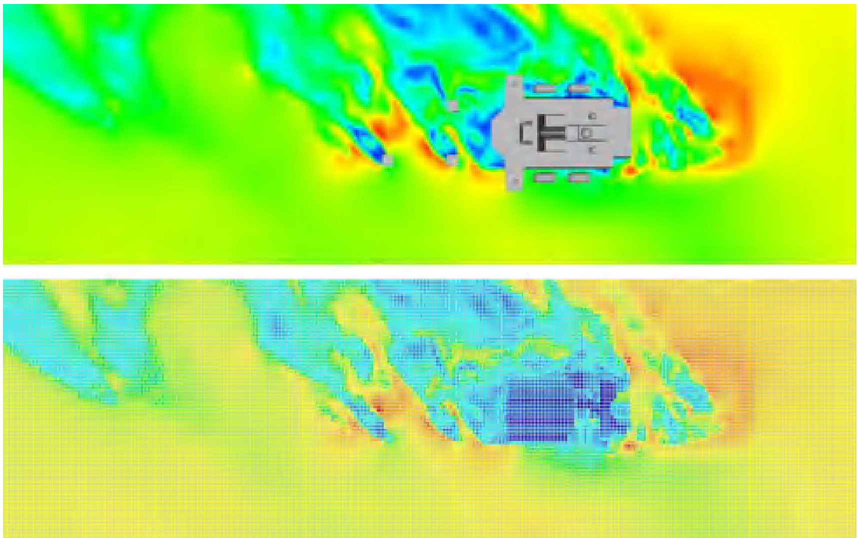

Fig. 8 Comparison of contours of longitudinal velocity component between raw CFD data (top) and interpolated airwake grid (bottom) for the Wave class AO at red 135 deg.

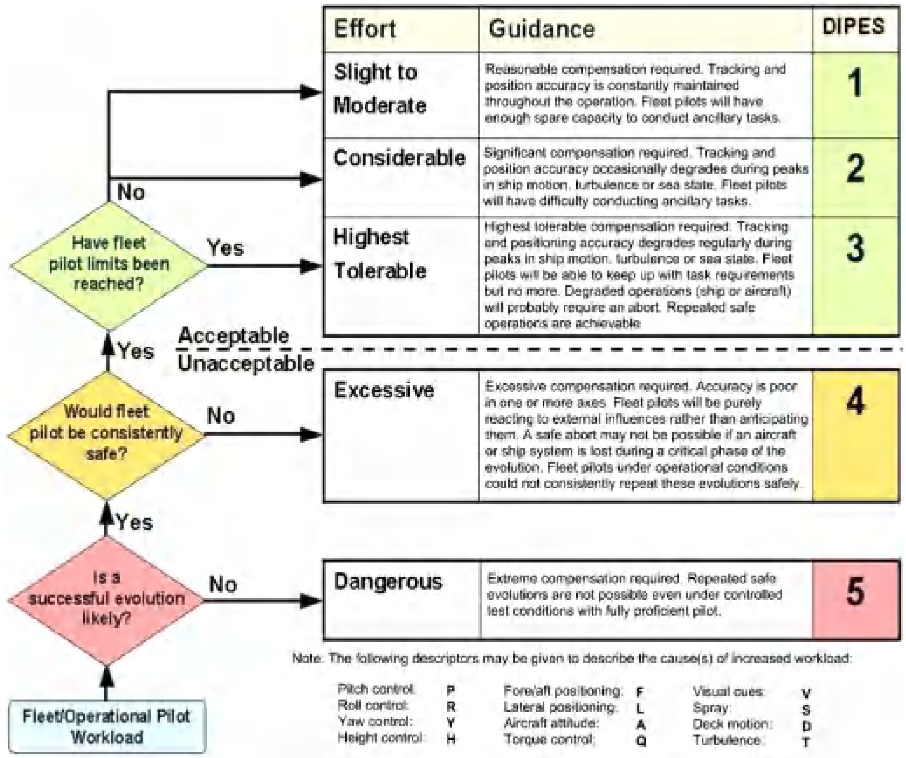

Fig. 10 The DIPES.

required; the three MTEs were therefore defined as 1) lateral translation across the deck to a hover over the landing spot; 2) a minimum of 10 s station keeping, in line with the hangar roof, over the landing spot; and 3) vertical descent to touchdown.

Following each deck landing the pilot gave subjective ratings, indicating the level of workload required during the task and the ability of an average fleet pilot to repeat the maneuver safely. The two ratings scales used were the DIPES and the Bedford workload rating scale (based on the Cooper–Harper handling qualities scale [34]); these scales are shown in Figs. 10 and 11 for reference. The pilot also provided verbal feedback on the difficulty of the task, the realism of the airwake turbulence and any other significant factors affecting performance; these comments were recorded alongside the ratings. In addition to the qualitative pilot workload ratings, activity from

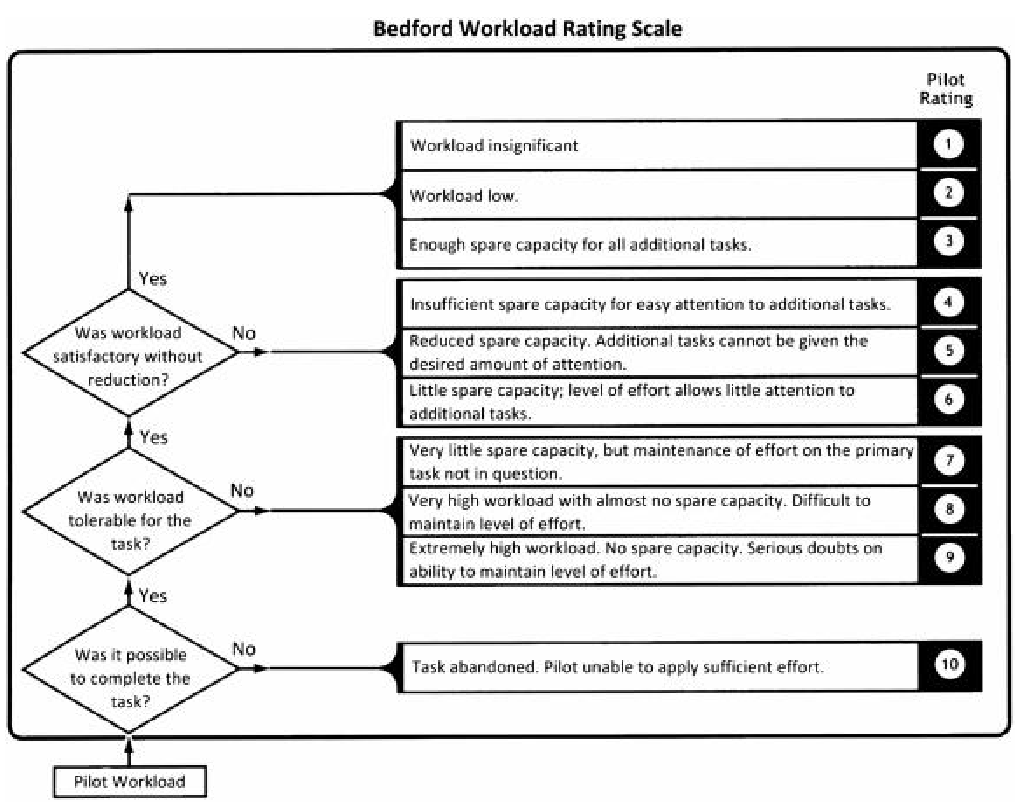

Fig. 11 The Bedford workload rating scale.

Table 2 WOD conditions tested for each ship during the piloted simulation flight trials

Ship	WOD angles, deg	WOD speeds	Velocity profile	Test points
SFS2	−15, 0, 15, 30, 45, 60, 90	20–50 kt	Uniform	19
Type 23 frigate	−15, 0, 15, 30, 45, 60, 90	25–50 kt	Uniform	21
Type 23 frigate	0, ±15, ±30, ±45, ±60, ±90	30–50 kt	ABL	34
Wave class AO	0, ±15, ±30, ±45, ±60, ±90	25–45 kt	ABL	28

each of the pilot's control inceptors was recorded for offline analysis. As well as giving an objective measure of how hard the pilot was working, these data were also used to determine whether the pilot was regularly exceeding control margins during the landing task. In accordance with commonly used DI test procedures (as described by Roscoe and Thompson in [7]), WOD conditions where the pilot consistently had less than 10% control margin remaining in any axis were assigned a DIPES rating of five.

As time with the test pilot was limited, the flight tests were planned such that test points where the airwake was expected to have an important effect were given priority. WOD conditions from red 15 deg to green 90 deg were tested first for each ship, with red 30 to 90 deg completed later if time allowed. Although winds from astern would normally be tested during at-sea SHOL trials, these are not usually limited by ship airwake turbulence, so were omitted from the simulated flight trials due to a lack of pilot time.

At each WOD angle, the pilot was given a 30 kt WOD speed as a first test point; this was then scaled up or down by either 5 or 10 kt for subsequent sorties, depending on the rating given at 30 kt. Once a DIPES rating of four was obtained for a given WOD angle, or if the pilot deemed it was not worth adding more WOD speed due to exceedance of control margins, a limit was found and the next WOD angle was loaded. The full test matrix achieved during the flight trials is shown in Table 2.

III. Piloted Flight Trial Results

A. General Observations and Subjective Pilot Comments

Figure 12 shows typical traces of the aircraft main rotor hub position plotted on a y-z plane, for several WOD angles which were obtained during several deck landing tasks. It can be seen that for the three cases presented the approach profiles are similar, and these are typical of the great majority of the landing tasks. The green 45 deg case shows slight deviation at the start of the maneuver, which is most likely due to the aircraft being subject to strong airwake turbulence in this off-deck location for that particular WOD condition. Figure 12 also illustrates a phenomenon which is observed at many of the red test points. For the red 15 deg case, as the aircraft approaches the port deck edge it gains several metres in height. This is due to an updraft caused as air passes up and over the port side of the flight deck. Pilot comments confirmed that this is realistic aircraft behavior for red winds.

Pilot comments were, generally, very favorable for the unsteady airwakes. In the majority of cases, where the aircraft was expected to encounter turbulence, the pilot commented that he experienced multi-axis disturbances. For example, at green 45 deg conditions the pilot observed strong turbulence alongside the deck which reduced in intensity as he traversed to hover over the landing spot. In contrast, for red winds very little turbulence was noticed alongside, with an increase in disturbances during station keeping. These observations were in good agreement with the pilot's experiences of at-sea deck landings.

Certain ship airwake phenomena are commonly experienced on approach to frigates for winds close to the bow. The so-called pressure wall effect and the effect of the aircraft being pulled towards the hangar have both been documented [9] and were also observed by the test pilot during these trials. The pressure wall requires the pilot to increase the lateral cyclic input as the aircraft approaches the deck edge in order to break through an invisible "wall"; as the aircraft punches through the wall, the aircraft accelerates laterally and reverse lateral cyclic is required to prevent overshoot. Although the cause of these phenomena is still not well understood, the fact that high-fidelity CFD airwakes are able to reproduce such realistic effects is encouraging. Indeed, it is hoped that simulated flight trials may lead to an improved understanding of these effects and provide valuable input to future ship superstructure design studies. Complimenting this, a further research study at the University of Liverpool is using experimental methods to investigate rotor response in airwake turbulence [35]; this is providing additional insight into the nature of ship airwake turbulence.

B. Fully Simulated Ship–Helicopter Operating Limits Envelopes

One of the key outcomes of this research project was the development of a simulation environment in which SHOL envelopes could be predicted before at-sea flight trials. Therefore, SHOL diagrams have been produced based on DIPES ratings given during the simulated landing tasks. In converting DIPES ratings to SHOL boundaries, ratings of 1–3 are deemed acceptable, while 4–5 are outside the SHOL (see Fig. 10). An important consideration for the DIPES scale is that ratings are given based on the perceived ability of an average fleet pilot, so although a highly capable test pilot may be able to safely land for a given WOD condition, a rating may be awarded which excludes that point from the envelope if it is deemed too difficult for a fleet pilot to perform on a regular basis.

Figure 13 presents the DIPES scores and the corresponding SHOL boundary for the two real ships. In construction of the SHOL boundaries a lateral velocity limit of 30 kt is assumed for the helicopter. This assumes that the critical flight condition for tail rotor authority is 35 kt sideways, allowing 5 kt side-slip into wind in case of overshoot. For both ships the lateral velocity limit results in a contraction of the SHOL on the red side. On the green side it was not necessary to artificially impose such a limit as the pilot either exceeded pedal control margins or deemed the task outside the SHOL due to the need for excessive amounts of right pedal.

Some major differences can be observed between the two ships, in terms of DIPES ratings and the resultant SHOL boundaries. All AO ratings are at least one DIPES point higher than the corresponding T23 ratings, and in many cases the difference is two. On a five-point rating scale these variances are significant. Both SHOL diagrams exhibit a similar shape; in general the SHOL boundary contracts on

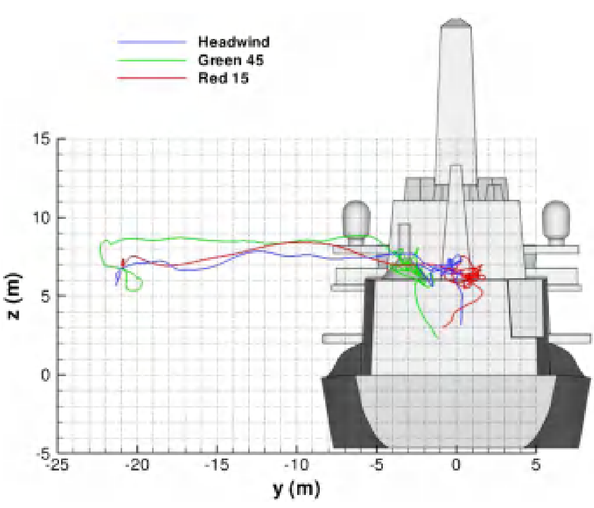

Fig. 12 Traces showing the position of the aircraft main rotor hub during the deck landing task for the Type 23 frigate at several WOD angles for 40 kt airwakes.

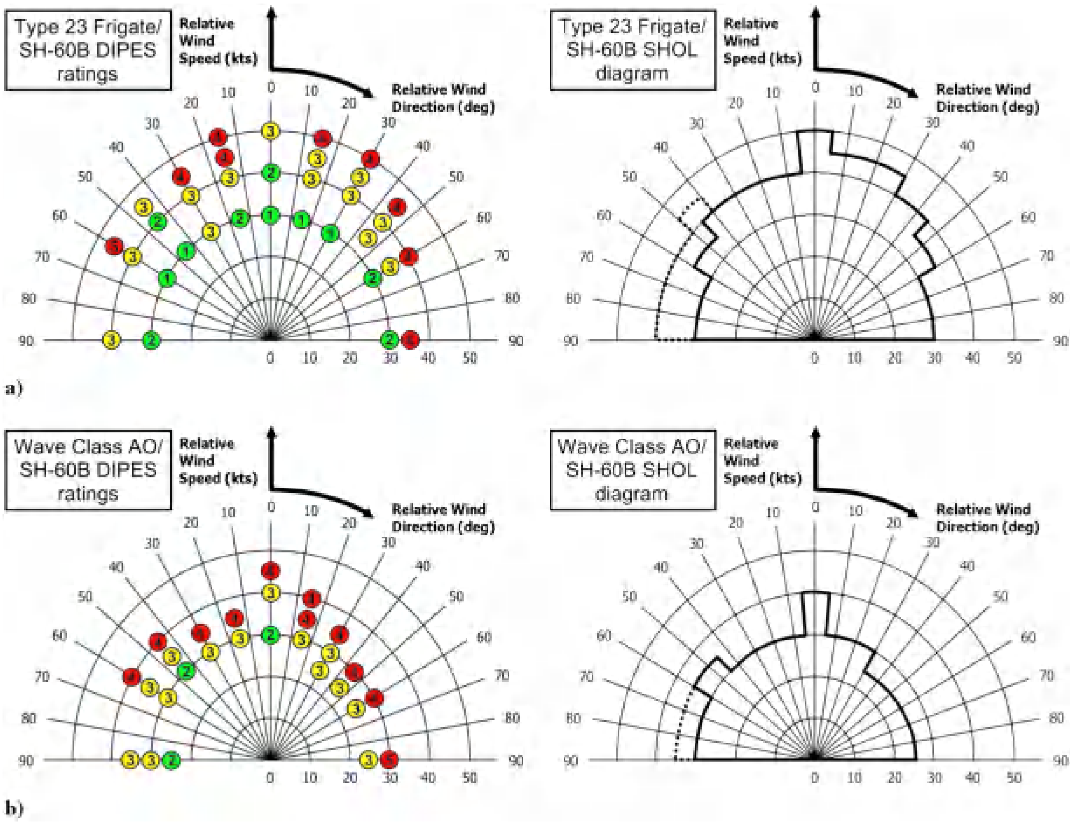

Fig. 13 DIPES ratings and SHOL diagrams for the a) Type 23 frigate and b) Wave class AO. The dashed line indicates the SHOL boundary purely from DIPES scores; the main boundary assumes a 30 kt lateral velocity envelope limit for the SH-60B.

either side of headwind, to a minimum at beam winds. However, the AO boundary is 5–15 kt lower than the T23 boundary at all locations except red 60 to 90 deg; this area is fixed due to the lateral velocity constraint.

An interesting feature is seen on the AO SHOL, where the boundary is seen to expand between red 45 to 60 deg. At these WOD conditions lower workload is experienced due to the fact that the aircraft is out of airwake turbulence for the majority of the deck landing. The windward hangar edge shear layer and turbulence shed from the superstructure are both swept away over the flight deck at an angle that has less impact on the helicopter than for winds closer to the bow. At these relatively low WOD speeds the tail rotor power requirements are not limiting, so the points are within the SHOL. A similar feature is seen at red 45 deg for the T23, but the point is prevented from being included due to the fact that the 45 kt WOD speed is outside the aircraft's lateral velocity envelope.

Although a methodology for deriving SHOL diagrams from CFD-based simulation has been presented, it has not been possible to compare the SHOL diagrams in Fig. 13 to any real SHOL diagrams for validation. Besides the fact that no SHOLs exist for the ship–helicopter combinations examined, SHOL charts for similar aircraft interfacing to these ships are working military documents and, as such, are restricted due to their sensitive nature. Although the authors are aware of a United Kingdom Ministry of Defence research programme comparing simulated SHOLs with at-sea data [8], there exists a need for more generic ship–helicopter flight-test data for the wider research community.

C. Ship Aerodynamics and Aircraft Handling Qualities

A valuable benefit of having team members both computing the CFD airwakes and conducting the flight trials is that in-depth knowledge of the ship aerodynamics can be used to gain insight into the aircraft handling qualities. Furthermore, the ability to return to the CFD results and interrogate the flow data using postprocessing tools allows the identification of flow features which may otherwise have been missed. This technique has been used to explain the cause of some specific phenomena observed during the simulated flight trials.

1. Effect of Ship Geometry

As discussed in the previous section, a difference in workload ratings was observed between the T23 and AO during the flight trials. At the 30 kt green 30 deg WOD condition, a DIPES rating of one was given for the T23 and three was awarded for the AO. Bedford workload ratings of four and three, and seven and five were given to the lateral translation and station keeping MTEs for the T23 and AO, respectively. Figure 14 shows the time history of airwake velocity components recorded at a location on the starboard side of the rotor disk (defined at 75% span, azimuth $\psi = 90$ deg) during the complete deck landing maneuver for the 30 kt green 30 deg test point, for both ships. The diagram is split into segments, each representing the approximate start and end time of each of the MTEs, with an extra MTE defined at the start of the sortie as an initial trim and stabilization phase before translation. It can be seen that the majority of airwake turbulence is encountered during the translation MTE, which is as expected, due to the aircraft passing through areas of highest turbulence during this phase. Figure 15 shows contours of turbulence intensity plotted at hangar height for both ships to illustrate this point.

Although the velocity traces shown in Fig. 14 are somewhat chaotic, the clear trend is that the AO disturbances are larger in magnitude than those seen from the T23. This applies to all three velocity components, with only the lateral component of the T23 airwake exhibiting perturbations close in magnitude to the AO airwake. It is also evident that the AO velocity fluctuations are more persistent during translation and station keeping than the T23. The CFD results shown in Fig. 15 suggest that this is most likely due to the fact that the wider superstructure of the AO prevents the aircraft from encountering clear, freestream air until much later in the maneuver. It can be seen that, in each axis, levels of turbulence intensity are higher and areas of high turbulence are larger for the AO compared to the T23.

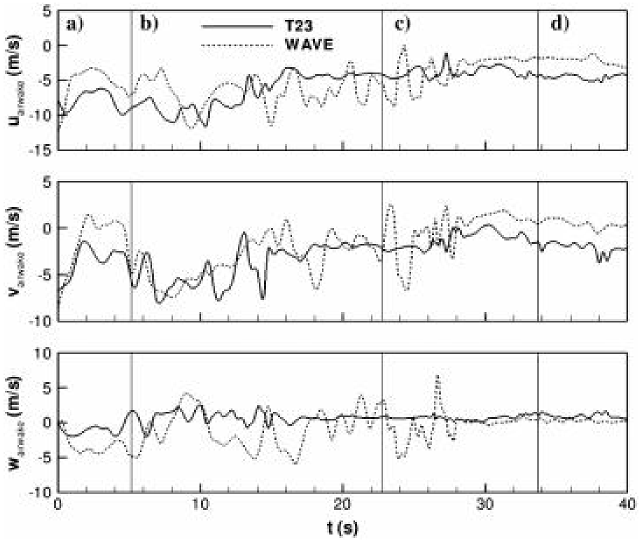

Fig. 14 Airwake velocity components recorded at a location on the starboard side of the rotor disk (defined at 75% span, azimuth $\psi = 90$ deg) during the deck landing task for the Type 23 frigate and Wave class AO (green 30 deg, 30 kt). Time histories are split into four MTEs: a) stabilized hover alongside ship, b) lateral translation across deck, c) station keeping over landing spot, and d) vertical landing.

In commenting on the differences between airwakes for the two ships, the pilot remarked that the AO airwake felt more "wallowy" than the T23, with lower frequency disturbances that were larger in magnitude. This required less frequent, but more severe corrections in order to maintain control of the aircraft. To investigate this further, the CFD airwake data were postprocessed by deriving power spectral density (PSD) plots from velocity time histories which were sampled at a point directly over the port side deck edge of both ships. The resulting data are plotted in Fig. 16, showing the frequency content of the airwakes. In each axis, and over the whole frequency range, the AO airwake contains more power than the T23 airwake, with significantly more in the vertical axis. This further confirms the discussion in the preceding paragraphs regarding the relative magnitude of airwake disturbances. Where peaks in the PSD plots exist for the two airwakes, the AO peak occurs at a lower frequency than the T23. For example, in the longitudinal axis a peak in the AO airwake is seen at approximately 0.3 Hz, with the T23 peak closer to 0.5 Hz. This is consistent with the pilot's comments regarding lower frequency disturbances during AO deck landings.

The relative size of the ships as shown in Fig. 5 can be related to the frequency shift observed in Fig. 16. It can be seen from Fig. 5 that the AO is significantly larger than the T23 and will therefore shed vortical structures which are larger than those shed from the T23 and, consistent with Strouhal scaling, will be shed less frequently. Similarly, for a given strength, larger vortices will induce higher velocities at their extremities. Both of these factors combine to suggest that, for ships with a conventional configuration (landing deck to stern behind a vertical hangar door), the airwake becomes more difficult to operate in with increasing size; although clearly

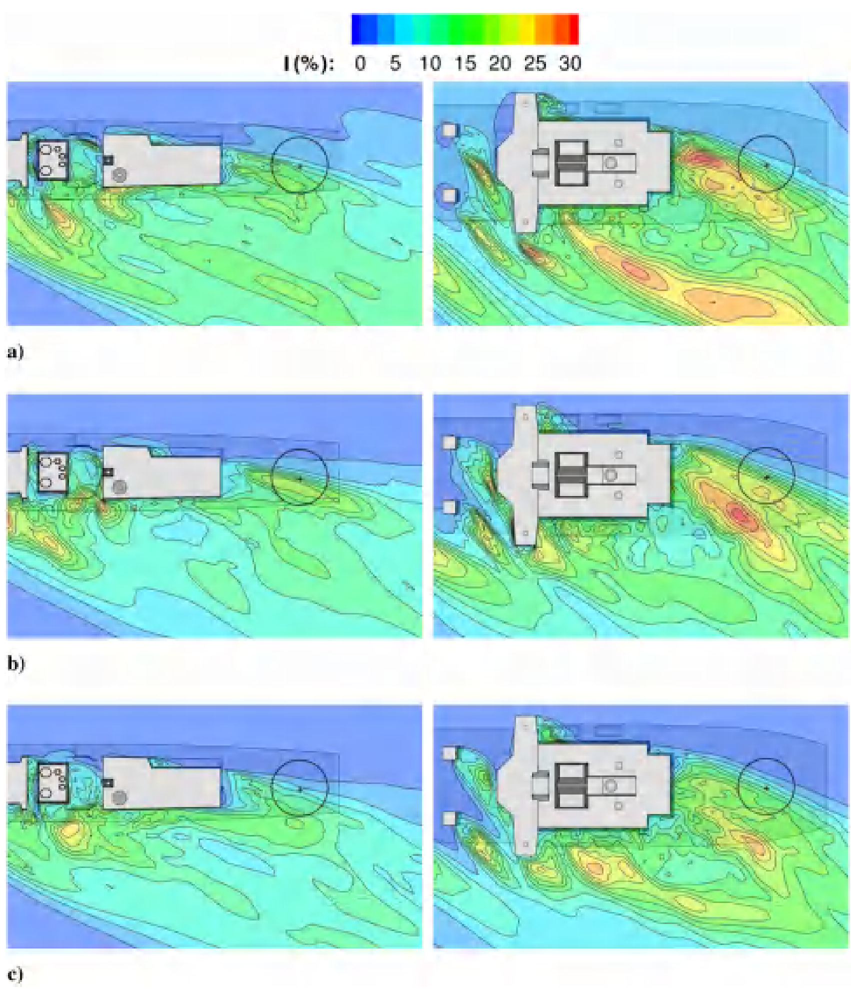

Fig. 15 Contours of turbulence intensity plotted at hangar height for the Type 23 frigate (left) and the Wave class AO (right) at green 30 deg. Longitudinal (a), lateral (b), and vertical (c) components are plotted, normalized by velocity magnitude at the anemometer height. The approximate location of the rotor disk during the station keeping task is denoted by the circle.

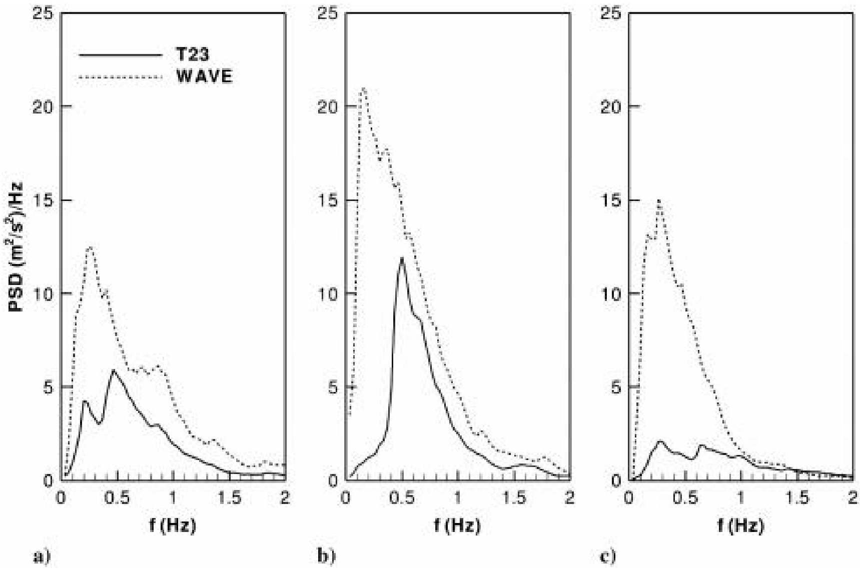

Fig. 16 PSD plots of Type 23 frigate and Wave class AO airwake velocity components at a location over the port side deck edge, in line with the landing spot, at hangar height (green 30 deg). Longitudinal (a), lateral (b), and vertical (c) components are shown.

small ships have their own operational limitations in terms of landing deck size and ship motion.

A further consideration in comparing workload ratings for different ships is the difference in visual cues available to the pilot. It was observed during the trials that the test pilot relied heavily on the natural horizon to maintain the aircraft in a level hover; the technique was described as “looking through the ship.” Behind the T23 hangar the pilot still had a reasonable view of the horizon, despite some superstructure partially blocking his view. However, the larger AO hangar and upwind superstructure almost totally blocked out the forward view of the horizon, leaving only a small region to the extreme port and starboard sides of his field of vision. It is possible that this disparity between visual cues may have contributed to the higher workload experienced during AO deck landings. This serves to highlight the complex interaction between cue environment, aircraft disturbances and pilot response which contribute to the difficulty of the shipboard landing task.

2. Effect of Wind-over-Deck Angle

It is clear from the DIPES ratings diagrams shown in Fig. 13 that winds either side of the headwind tend to cause increased workload. This is mainly due to the effects of shear layers and vortices which strengthen as the wind angle becomes more oblique; these flow features being the primary mechanisms for airwake turbulence generation. It was anticipated that results from the deck landing trials would be able to provide a better understanding of how these turbulent airwake features drive pilot workload and control strategy at different WOD angles. For the purposes of this study it was convenient to choose two WOD conditions which were given significantly different workload scores by the pilot, as a contrast in workload rating should also indicate a dissimilar airwake structure. Therefore, it was decided that the T23 headwind and green 45 deg WOD angles would be analyzed, both for WOD speeds of 40 kt. For the station keeping task the test pilot gave the headwind case a Bedford workload rating of 4, classified as “Insufficient spare capacity for easy attention to additional tasks.” The green 45 deg case was given a rating of 6, classified as “Little spare capacity; level of effort allows little attention to additional tasks.” It is instructive to look at a visualization of the flowfields at the chosen WOD angles in order to determine what may be causing the differences in workload. Figure 17 shows contours of turbulence intensity on a plane at 6 m above the flight deck. A marked difference in flowfields can be seen. For the headwind, turbulence is moderate over the whole of the flight deck, whereas the green 45 deg case shows a flight deck bisected by a region of high turbulence which is shed from the windward hangar edge. Although at green 45 deg much of the velocity field experienced by the rotor disk is at freestream conditions, the region between 180 and 330 deg azimuth (counter-clockwise from the rear of the disk) is subjected to levels of airwake turbulence with peak vertical velocity magnitudes up to 75% higher than the headwind case.

Figure 18 largely confirms the pilot’s assertion that he was working harder during the green 45 deg landing, showing PSD plots

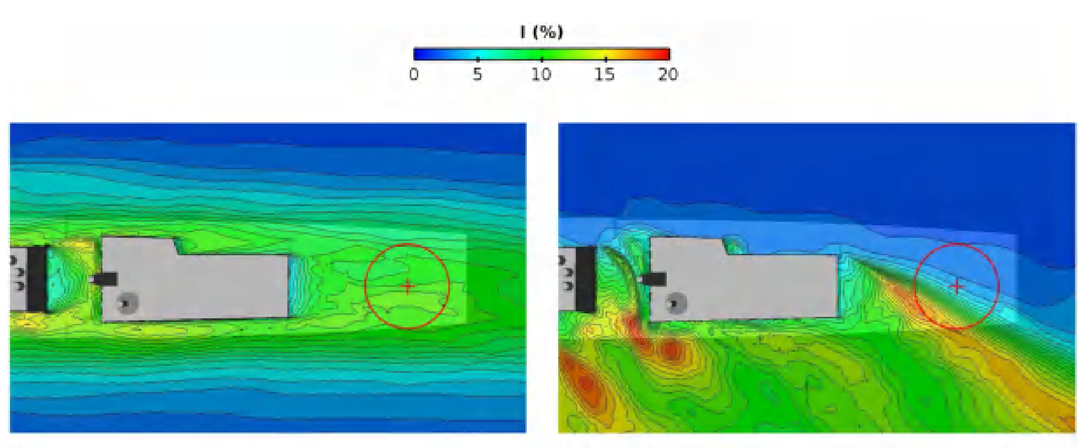

Fig. 17 Contours of turbulence intensity plotted at a height of 6 m above the flight deck. The approximate location of the rotor disk during the station keeping task is denoted by the circle: a) headwind and b) green 45 deg.

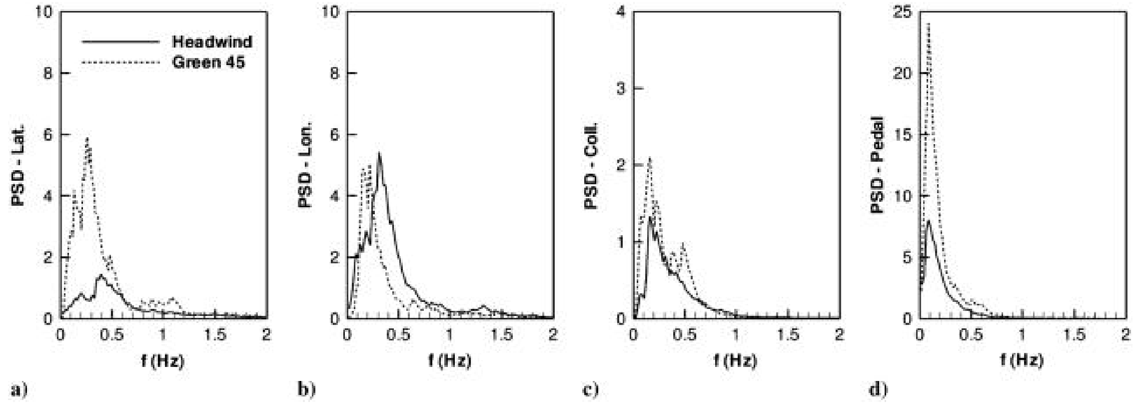

Fig. 18 PSD plots of pilot control activity during the deck landing task for the 40 kt headwind and green 45 deg cases (PSD values have been normalized by 1×10^{-3} for clarity). Diagrams show, from left to right, lateral cyclic, longitudinal cyclic, collective, and pedal.

for each of the control axes derived from time histories of pilot control inputs. In all axes except the longitudinal cyclic the PSD levels are significantly higher for the green 45 deg case than for the headwind. It can be seen that all activity is to the lower end of the typical 0.2–2 Hz pilot closed-loop response range. The very large low-frequency peak seen for the pedal activity in the green 45 deg case is likely to be exaggerated due to the gradual application of left pedal during the lateral translation into freestream conditions; when data from just the station keeping MTE is isolated and plotted a smaller peak is observed, but this is still significantly higher in magnitude than the headwind data. For the green 45 deg cases the pilot consistently reported pedal activity as being a dominant factor in terms of workload. For the cyclic, similar levels of activity are seen in both axes during the green 45 deg test point, with slightly more in the lateral channel. In contrast, for the headwind case there is very little activity in the lateral axis, with a marked increase in longitudinal activity, comparable in magnitude to the green 45 deg case.

Although the contours of turbulence intensity shown in Fig. 17 give an indication of which regions are likely to experience large fluctuations, they give no indication about the instantaneous perturbations. Figure 19 shows contours of instantaneous vertical velocity at an estimated rotor disk location during the station keeping task, for both WOD conditions. The vertical axis was chosen as it is well known that the vertical velocity component is important in causing rotor disk disturbances, by changing the induced velocity distribution and hence the effective angle of attack of the blades [36]. The headwind case on the left side shows that there are moderate spatial velocity variations and pilot comments suggest that some airwake turbulence at the headwind condition was felt, but it was at a magnitude which was manageable, hence the Bedford score of 4. In

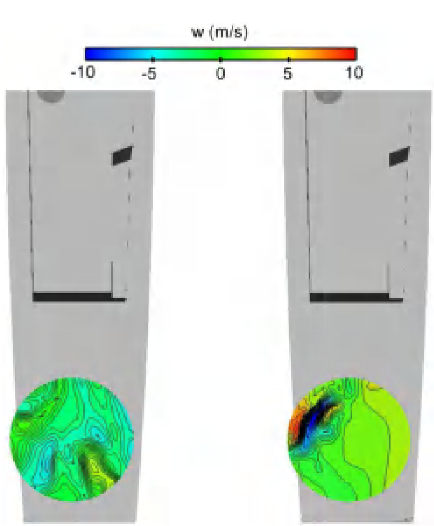

Fig. 19 Contours of instantaneous vertical velocity plotted at the approximate location of the rotor disk during the station keeping task, for the 40 kt headwind (left) and green 45 deg (right) cases.

contrast, the right side of Fig. 17 shows high vertical velocities, both positive and negative, on the rotor disk between approximately 210 and 290 deg azimuth; the most severe gradient occurs at approximately 270 deg. When animated, these large-amplitude perturbations are seen to convect across the disk at a lower frequency than the lower-amplitude headwind turbulence. It appears that the frequency and magnitude of the green 45 deg turbulence shed from the starboard hangar edge are the main drivers for workload at this condition. The pilot commented that it was easier to make constant, small adjustments to the controls than to be hit suddenly with large disturbances that required more extreme control inputs, hence the higher ratings for the green 45 deg case; again, these comments concur with the underlying CFD data.

IV. Conclusions

A ship–helicopter DI flight simulation facility based at the University of Liverpool has been described, which allows simulated deck landings to be conducted under the influence of realistic unsteady ship airwakes. The airwake perturbations are provided by aerodynamic look-up tables which have been populated by offline CFD computations of the air flow over several ships at various WOD angles. Simulated flight trials have been conducted to mimic, as far as possible, at-sea FOCFT testing; this has so far been limited to the deck landing part of the ship–helicopter interface. DIPES ratings taken from a highly experienced test pilot have been used to construct, the first known published, fully simulated SHOL diagrams.

Pilot comments regarding the simulated flying experience were, generally, very good. The pilot reported feeling the effects of turbulence in locations where it was expected. For example, at a green 45 deg WOD condition, turbulence was encountered to the port side of the flight deck in the lee of the superstructure, but not to the starboard side of the deck. Other phenomena, such as the so-called pressure wall and updraft over the port side deck edge for red winds, were also observed.

The ability to return to the CFD and use the underlying aerodynamic data as a tool for understanding certain flight-test results was shown to be a key aspect of this methodology. Differences in airwake severity were observed between the T23 and AO, leading to a more restrictive SHOL for the AO. Aerodynamic data suggested that this was due to the relative size of the ships leading to airwakes with differing frequency content. Similarly, the increase in reported workload as winds move from ahead around to green 45 deg were attributed to the difference in the structure of the airwake and the increasing strength of turbulent structures as winds become more oblique.

The simulation methodology described in this paper was conducted using virtual models (ship CAD data, aircraft flight model) throughout, lending itself well to virtual prototyping. In particular, with ships still at the design stage, this type of DI simulation approach could be a valuable tool to assess the structure and severity of the expected ship airwakes, and their potential impact on ship–helicopter operations.

Acknowledgments

The authors would like to acknowledge financial support from Westland Helicopters, Defence Science and Technology Laboratory, and the ongoing support from Engineering and Physical Sciences Research Council. ANSYS, Inc., have also provided valuable assistance. The first author is employed by the Virtual Engineering Centre, which is a University of Liverpool project partially funded by North-West Development Agency and European Regional Development Fund located at the Daresbury Laboratory of the Science and Technology Facilities Council. The authors would like to thank the test pilot, Andy Berryman, for his professionalism and guidance. Many hours of help and support have also been given by Philip Perfect, Neil Cameron, and Mark White from the University of Liverpool's Flight Science and Technology research group. Cliff Addison helped immensely with the computing cluster setup and maintenance.

References

[1] Carico, D., Fang, R., Finch, R. S., Geyer, W. P., Jr., Krijns, H. W., and Long, K., "Helicopter/Ship Qualification Testing," RTO/NATO, TR RTO-AG-300-V22, 2003.

[2] Advani, S. K., and Wilkinson, C. H., "Dynamic Interface Modelling and Simulation: A Unique Challenge," Royal Aeronautical Society Conference on Helicopter Flight Simulation, London, Nov. 2001.

[3] Blackwell, J., Arney, A. M., Gilbert, N. E., and Truong, T. T., "Modelling the Helicopter/Ship Dynamic Interface for the Seahawk/FFG-7," Australian Aeronautical Conference, Proceedings No. 93/6, Institution of Engineers, Australia, Sept. 1993.

[4] Erm, L. P., "A Preliminary Study of the Airwake Used in an Existing SH-60B/FFG-7 Helicopter/Ship Simulation Program," DSTO, TR DSTO-TR-0015, 1994.

[5] Wilkinson, C., Zan, S., Gilbert, N., and Funk, J., "Modelling and Simulation of Ship Air Wakes for Helicopter Operations: A Collaborative Venture," AGARD Symposium on Fluid Dynamics, Problems of Vehicles Operating Near or in the Air–Sea Interface, Amsterdam, 5–8 Oct. 1998.

[6] Bunnell, J. W., "An Integrated Time-Varying Airwake in a UH-60 Black Hawk Shipboard Landing Simulation," AIAA Modeling and Simulation Technologies Conference and Exhibit, Montreal, 6–9 Aug. 2001.

[7] Roscoe, M. F., and Thompson, J. H., "JSHIP's Dynamic Interface Modeling and Simulation System: A Simulation of the UH-60A Helicopter/LHA Shipboard Environment Task," American Helicopter Society 59th Annual Forum, Phoenix, AZ, 6–8 May 2003.

[8] Cox, I. G., and Duncan, J. M., "Optimising the Ship/Air Vehicle Interface via Simulation," Royal Institution of Naval Architects International Conference: Warship 2009: Airpower at Sea, London, 17–18 June 2009, pp. 53–62.

[9] Zan, S. J., "On Aerodynamic Modelling and Simulation of the Dynamic Interface," Proceedings of the Institution of Mechanical Engineers, Part G: Journal of Aerospace Engineering, Vol. 219, No. 5, 2005, pp. 393–410.
doi:10.1243/095441005X30315

[10] Tai, T. C., and Carico, D., "Simulation of DD-963 Ship Airwake by Navier–Stokes Method," Journal of Aircraft, Vol. 32, No. 6, 1995, pp. 1399–1401.
doi:10.2514/3.46892

[11] Landsberg, A. M., Young, T. R., Jr, and Boris, J. P., "Analysis of the Nonlinear Coupling Effects of a Helicopter Downwash with an Unsteady Ship Airwake," 33rd AIAA Aerospace Sciences Meeting and Exhibit, Reno, NV, 9–12 Jan. 1995.

[12] Landsberg, A. M., Sandberg, W. C., Young, T. R., and Boris, J. P., "DDG-51 Flt-IIA Airwake Study Part 2: Hangar Interior Flow," Naval Research Lab., TR NRL/MR/6410-96-7898, 1996.

[13] Liu, J., Long, L. N., and Modi, A., "Higher Order Accurate Solutions of Ship Airwake Flow Fields Using Parallel Computer," American Helicopter Society 54th Annual Forum, Washington, D.C., 20–22 May 1998, pp. 58–70.

[14] Polsky, S. A., and Bruner, C. W. S., "Time-Accurate Computational Simulations of an LHA Ship Airwake," 18th AIAA Applied Aerodynamics Conference, Denver, CO, 14–17 Aug. 2000.

[15] Reddy, K. R., Toffoletto, R., and Jones, K. R. W., "Numerical Simulation of Ship Airwake," Computers and Fluids, Vol. 29, No. 4, 2000, pp. 451–465.
doi:10.1016/S0045-7930(99)00033-X

[16] Sharma, A., and Long, L. N., "Airwake Simulations on an LPD-17 Ship," AIAA Paper 2001-2589, 2001.

[17] Polsky, S. A., "A Computational Study of Unsteady Ship Airwake," 40th AIAA Aerospace Sciences Meeting and Exhibit, Reno, NV, 14–17 Jan. 2002.

[18] Polsky, S. A., "CFD Prediction of Airwake Flowfields for Ships Experiencing Beam Winds," 21st AIAA Applied Aerodynamics Conference and Exhibit, Orlando, FL, 23–26 June 2003.

[19] Syms, G. F., "Numerical Simulation of Frigate Airwakes," International Journal of Computational Fluid Dynamics, Vol. 18, No. 2, 2004, pp. 199–207.
doi:10.1080/10618560310001634159

[20] Lee, D., Sezer-Uzol, N., Horn, J. F., and Long, L. N., "Simulation of Helicopter Shipboard Launch and Recovery with Time-Accurate Airwakes," Journal of Aircraft, Vol. 42, No. 2, 2005, pp. 448–461.
doi:10.2514/1.6786

[21] Lee, D., and Horn, J. F., "Simulation of Pilot Workload for a Helicopter Operating in a Turbulent Ship Airwake," Proceedings of the Institution of Mechanical Engineers, Part G: Journal of Aerospace Engineering, Vol. 219, No. 5, 2005, pp. 445–458.
doi:10.1243/095441005X30298

[22] Sezer-Uzol, N., Sharma, A., and Long, L. N., "Computational Fluid Dynamics Simulations of Ship Airwake," Proceedings of the Institution of Mechanical Engineers, Part G: Journal of Aerospace Engineering, Vol. 219, No. 5, 2005, pp. 369–392.
doi:10.1243/095441005X30306

[23] Roper, D. M., Owen, I., Padfield, G. D., and Hodge, S. J., "Integrating CFD and Piloted Simulation to Quantify Ship-Helicopter Operating Limits," Aeronautical Journal, Vol. 110, No. 1109, 2006, pp. 419–428.

[24] Forrest, J. S., Hodge, S. J., Owen, I., and Padfield, G. D., "An Investigation of Ship Airwake Phenomena Using Time-Accurate CFD and Piloted Helicopter Flight Simulation," 34th European Rotorcraft Forum, Liverpool, England, U.K., 16–19 Sept. 2008.

[25] Forrest, J. S., and Owen, I., "An Investigation of Ship Airwakes Using Detached-Eddy Simulation," Computers and Fluids, Vol. 39, No. 4, 2010, pp. 656–673.
doi:10.1016/j.compfluid.2009.11.002

[26] Forrest, J. S., Owen, I., Padfield, G. D., and Hodge, S. J., "Detached-Eddy Simulation of Ship Airwakes for Piloted Helicopter Flight Simulation," First International Aerospace CFD Conference, Paris, 18–19 June 2007.

[27] Forrest, J. S., Hodge, S. J., Owen, I., and Padfield, G. D., "Towards Fully Simulated Ship-Helicopter Operating Limits: The Importance of Ship Airwake Fidelity," American Helicopter Society 64th Annual Forum, Vol. 1, Montreal, 29 April–1 May 2008, pp. 339–351.

[28] White, M., Perfect, P., Padfield, G., Gubbels, A., and Berryman, A., "Acceptance Testing of a Rotorcraft Flight Simulator for Research and Teaching: The Importance of Unified Metrics," 35th European Rotorcraft Forum, Hamburg, Germany, 21–25 Sept. 2009.

[29] Perfect, P., White, M., Padfield, G., Gubbels, A., and Berryman, A., "Predicting Simulator Fidelity through ADS-33 Metrics," 36th European Rotorcraft Forum, Paris, 7–9 Sept. 2010.

[30] Manimala, B., Walker, D., and Padfield, G., "Rotorcraft Simulation Modelling and Validation for Control Design and Load Prediction," 31st European Rotorcraft Forum, Florence, Italy, 13–15 Sept. 2005.

[31] Spalart, P. R., Jou, W. H., Strelets, M., and Allmaras, S. R., "Comments on the Feasibility of LES for Wings, and on a Hybrid RANS/LES Approach," Advances in DNS/LES, Greyden, 1997, pp. 137–147.

[32] Counihan, J., "Adiabatic Atmospheric Boundary Layers: A Review and Analysis of Data from the Period 1880–1972," Atmospheric Environment, Vol. 9, No. 10, 1975, pp. 871–905.
doi:10.1016/0004-6981(75)90088-8

[33] Fang, R., Krijns, H. W., and Finch, R. S., "Dutch/British Clearance Process," RTO AGARDograph 300: Helicopter/Ship Quali*fi*cation Testing, edited by G. D. Carico, R. Fang, R. Finch, W. P. Geyer, Jr., H. W. Krijns, and K. Long, Vol. 22, Flight Test Techniques Series, NATO Research and Technology Organization, 2003.

[34] Roscoe, A. H., and Ellis, G. A., "A Subjective Ratings Scale for Assessing Pilot Workload in Flight: A Decade of Practical Use," RAE, TR TR90019, 1990.

[35] Kääriä, C. H., Wang, Y., Curran, J., Forrest, J., and Owen, I., "AirDyn: An Airwake Dynamometer for Measuring the Impact of Ship Geometry on Helicopter Operations," 36th European Rotorcraft Forum, Paris, 7–9 Sept. 2010.

[36] Padfield, G. D., Helicopter Flight Dynamics, 2nd ed., Blackwell Science, Boston, 2007.